An improved energy-efficient driving strategy for routes with various gradients and speed limits

Liu, Xiao; Tian, Zhongbei; Jiang, Lin; Lu, Shaofeng; Zeng, Pingliang

DOI:
10.1049/itr2.12482

Received: 25 August 2023 | Revised: 16 December 2023 | Accepted: 12 January 2024

IET Intelligent Transport Systems

DOI: 10.1049/itr2.12482

The Institution of Engineering and Technology WILEY

ORIGINAL RESEARCH

An improved energy-efficient driving strategy for routes with various gradients and speed limits

Xiao Liu[1] | Zhongbei Tian[2] | Lin Jiang[1] | Shaofeng Lu[3] | Pingliang Zeng[4]

[1]Department of Electrical Engineering and Electronics, University of Liverpool, Liverpool, UK

[2]School of Engineering, University of Birmingham, Birmingham, UK

[3]Shien-Ming Wu School of Intelligent Engineering, South China University of Technology, Guangzhou, China

[4]School of Automation, Hangzhou Dianzi University, Hangzhou, China

Correspondence
Zhongbei Tian, School of Engineering, University of Birmingham, Birmingham B15 2TT, UK.
Email: z.tian@bham.ac.uk

Abstract

With the increasing concerns about railway energy efficiency, two typical driving strategies have been used in actual train operation. One includes a sequence of full power traction, cruising, coasting, and full braking (CC). The other uses coasting–remotoring (CR) to replace cruising in CC. However, energy-saving performance by CC and CR, which can be affected by route parameters of gradients and speed limits, has not been fully compared and studied. This paper analyses the energy distribution of CC and CR considering various route parameters and proposes an improved strategy for different gradients and speed limits. The detailed energy flow of CC and CR is analysed by Cauchy–Bunyakovsky–Schwarz inequality and the generalised Hölder's inequality, and then, a novel driving strategy CC_CR is designed. To verify the theoretical results and the effectiveness of the proposed strategy, three simulators with CC, CR, and CC_CR driving modes have been developed and implemented into case studies of four scenarios as well as a real-world metro line. Simulation results demonstrate that CR can only outperform CC on routes with steep downhill and CC_CR is always the best strategy. The energy savings of CC_CR can be as much as 15% more than CR and 42% greater than CC.

1 | INTRODUCTION

Energy shortage has become a global issue, particularly in recent years. The price of energy has risen a lot because of its scarcity. Although the railway is one of the most energy-efficient transport, it still consumes a large amount of energy every day. So, the research on how to improve the energy efficiency of railway systems is of great significance. Train trajectory optimisation as a low-cost, flexible, and easy-to-implement method to reduce the energy consumption of railway systems has attracted the attention of many researchers.

The train trajectory optimisation methods are usually divided into direct exact, indirect exact, and heuristic methods [1]. Direct exact solution method works by discretising the train operation process first, and then changing the problem into a static non-linear programming problem. In recent years, dynamic programming (DP), mixed linear programming (MILP), and pseudospectral method have been applied to solve this problem. Reference [2] developed a distance-based DP and compared it with two heuristic algorithms genetic algorithm (GA) and Ant colony algorithm (ACO). This paper showed the effectiveness of DP in solving the train trajectory optimisation problem, but also pointed out that it may suffer from 'curse of dimension' when the solution space increases. In [3], the mixed integer linear programming (MILP) model is built to find the optimal solution for part of the train speed profile. MILP was also utilised by [4] to address the train trajectory optimisation problem while considering the discrete throttle settings, neutral zones, and sectionalized tunnel resistance of high-speed railway. Reference [5] first introduced pseudospectral method to solve the energy-efficient train control problem and compared the result with MILP, which shows that the energy saving of this method is better than MILP, but more computational time is needed. However, despite the long computational time, pseudospectral optimisation also suffers from oscillation of the solution on the singular control phases [6]. In contrast, the indirect method can avoid these problems. This method is usually based on the Pontryagin maximum principle (PMP) analysis, which concluded that on non-steep tracks, the optimal train

driving sequence is full power traction–cruising–coasting–full braking [7, 8].

Based on the PMP result, many papers consider the energy-efficient train control problem as finding the optimal switching points between the four optimal driving regimes. Such a method is referred to as CC (cruising–coasting) strategy in this paper. The CC strategy has been studied by many researchers in these years. Reference [9] created a Driver Practical Training System to determine when to switch between cruising and coasting using an enhanced Brute Force searching algorithm. In [10], Fibonacci algorithm and bisection method were introduced to obtain the optimal cruising and coasting speed. Taking the passenger points into consideration, [11] introduced the DP method to search for the optimal switching points. Reference [12] developed a real-time driver advisory system for the high-speed railways by finding the optimal costing regimes. An improved brute-force search algorithm was introduced by [13] to find the optimal switching positions. Heuristic searching algorithms such as GA [14] and hybrid evolution algorithm [15] are also used to solve the optimal switching points searching problem. Reference [16] considered the section running time constraint by adding another traction–cruising–coasting into the CC speed profile. However, the steep hills are not considered in these publications. Although [17, 18] formulated the mathematical model by considering steep hills in particularly, the problem is hard to solve when it comes to practical route with complex speed limits and gradients.

Different from the CC method, there is another driving strategy called CR (coasting–remotoring), which does not include cruising in the driving process. The speed is maintained by coasting-remotoring pairs. This method can use coasting to save energy during train operation instead of only coasting before braking. Reference [19] compared GA and hierarchical GA in searching the switching points between coasting and remotoring, which concluded that the GA could only be applied when the number of coasting points is pre-determined. In contrast, the hierarchical GA can determine the number and position of the coasting points but cannot guarantee a fitter solution in certain traffic conditions. As an extension of [19], [20] applied this method on multiple trains to find the most energy-efficient speed profiles. While taking the acceleration and deceleration rates as control variables, [21] employed GA to derive the most energy-efficient upper and lower bounds. Additionally, to optimise the ATO (Automatic Train Operation system) speed profile of the Madrid underground, [22] used the multi-objective particle swarm optimisation search algorithm to find the most energy-efficient cruising speed or upper and lower bounds of CR (only one dominated mode for an interstation). In [23], the particle swarm and GA were combined to optimise the speed profile under the prerequisite that the train speed profile is composed of a series of coasting-remotoring or coasting-braking. Reference [24] applied the Karush–Kuhn–Tucker conditions to develop equations, the solutions of which define the upper and lower speed limits for coasting-remotoring pairs. Similar to the CR driving strategy, [25] obtained the optimal sequence of coasting, full power motoring, or partial braking during the trip by using a soft actor-critic-based method. Furthermore, [26] introduced MILP to optimise the cyclic air braking on long steep downhills for heavy-haul trains.

There are notable distinctions between CC and CR driving strategies. Firstly, CC relies on precise speed profile tracking devices, especially for achieving optimal results during cruising. In contrast, CR is relatively straightforward to implement, requiring action only when predefined speed values are reached. Secondly, CC excels in passenger comfort compared to CR. However, when evaluating their energy-saving performance, a more in-depth analysis is needed. This study will serve as the foundation for exploring the integration of CC's and CR's advantages into a single strategy. Based on the description above, the current research gap can be summarised as follows:

(1) CC and CR-based studies only compare their optimisation results with the non-optimised ones or the same driving strategy under different optimisation algorithms. No theoretical investigation into the distinction between CC and CR has been carried out. For example, [9, 11, 12, 15] only concentrated on the algorithms to search the optimal switching points, and [10, 27, 28] expanded the model by considering timetable, transmission loss, and mechanical wear, or engine shutdown during cruising. Similarly, CR-based research only focused on the methods to find the optimal upper and lower control bounds [19–23, 29, 30].
(2) Few studies have combined CC and CR in one speed profile. Although [31, 32] considered CC and CR in one optimisation problem, the two strategies are actually independent. Cruising and coasting-remotoring cannot appear in one optimal strategy at the same time. Additionally, the conditions when CC or CR will appear in the optimisation results have not been analysed. In [33], the optimal speed profile includes cruising and coasting-remotoring. But the number of these regimes is pre-defined, and how to find a reasonable number has not been considered.
(3) In reality, more than one optimal speed profile with different running times are usually needed to meet the peak and off-peak time requirement, as well as to deal with unexpecting disturbance [34]. Therefore, it is essential to calculate energy usage over various operating times to assess a method's efficacy. This requirement is reflected in the acquisition of the Pareto frontier, which delineates the trade-off between travel time and energy consumption as documented in sources [22, 33, 35, 36]. However, a comparative analysis of the Pareto frontiers for CC and CR remains unexplored.

To fill the research gaps explained above, and make full use of the advantages of CC and CR, this paper investigates the performance of CC and CR on routes with various gradients and speed limits and develops a new energy-efficient train control strategy that can combine the advantages of these two strategies. The main contributions of this paper are

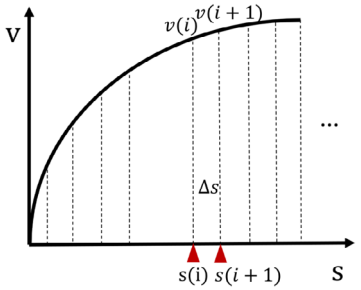

FIGURE 1 Discretisation of the journey.

- Introduce the Cauchy–Bunyakovsky–Schwarz inequality and the generalised Hölder's inequality to analyse the energy distribution of CC and CR on single gradient and speed limit
- Develop an improved energy-efficient train control strategy combining the advantages of CC and CR. In this strategy, the numbers of cruising-coasting and coating-remotoring are also adjusted to obtain the most energy-efficient trajectory under various running times.
- Verify the energy distribution analysis and energy-saving performance of CC, CR, and CC_CR by comparing their Pareto frontiers in four route scenarios.

The rest of this paper is organised as follows. In Section 2, train operation models and the control strategies CC and CR are introduced. In Section 3, the influence of gradient and speed limit on energy consumption with different driving strategies is analysed. In Section 4, an improved energy-efficient train driving strategy, CC_CR is developed. In Section 5, case studies of applying CC, CR, and CC_CR in four scenarios are presented. Finally, the conclusions of this paper are drawn.

2 | TRAIN OPERATION MODELLING

2.1 | Train dynamics

The train motion can be discretised by a distance interval Δs as shown in Figure 1. i is the distance index. $v(i)$ and $s(i)$ are the speed and distance at the ith step.

The relationship between $v(i)$ and $v(i+1)$ is represented by Equation (1). The speed at the start of the journey is $v(1) = 0$. The acceleration $a(i)$ is calculated by Equation (2).

$$2a(i)\Delta s = v(i+1)^2 - v(i)^2 \tag{1}$$

$$a(i) = \frac{F(i) - R(i) - G(i)}{(1+\lambda)M} \tag{2}$$

where $F(i)$ is the tractive or braking effort, $R(i)$ is vehicle resistance, $G(i)$ is the component effort of gravity in or opposite to the direction of train motion, λ is the rotary allowance, M is the mass of the rolling stock. The value of $F(i)$ is bounded by a maximum electrical tractive effort curve and a maximum electrical braking effort curve which depend on the train speed.

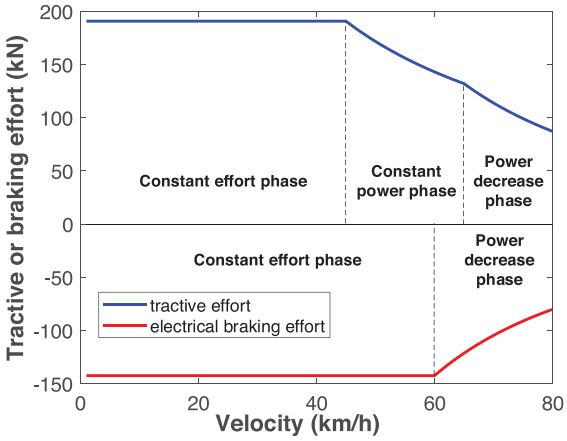

FIGURE 2 Maximum effort on a vehicle.

A typical pair of maximum traction and braking curves are shown in Figure 2. In this figure, the maximum tractive effort includes three phases: constant effort phase, constant power phase, and power decrease phase. But the maximum electrical braking curve only has constant effort and braking power decrease phase.

The rolling resistance and component effort of gravity in Equation (2) are calculated by Equations (3) and (4).

$$R(i) = A + Bv(i) + Cv(i)^2 \tag{3}$$

$$G(i) = Mg \times grad(i) \tag{4}$$

where A, B, and C are Davis constants [37], which are determined by the attributes of the rolling stocks, g is the acceleration due to gravity, and $grad(i)$ is the gradient at the ith step.

2.2 | CC driving mode

CC consists of full power traction, cruising, coasting, and the final full braking. The full power traction is active at the start of the journey to increase the vehicle's speed. Here full power means using the maximum tractive effort shown in Figure 2. Cruising regime is applied when the train reaches a certain speed. When the train is cruising, the resultant force is zero. In the coasting regime, no tractive or braking effort is required. The acceleration of the train is only caused by resistance and gradient. Full braking is applied before a speed limit decrease or the end of the journey. The cruising speeds (V_cr) and coasting speeds (V_co) vary in different speed limit sections as in [35]. The CC train speed profile is illustrated in Figure 3.

2.3 | CR driving mode

In the CR control strategy, one pair of control speeds, namely the upper bound and lower bound are set for every speed limit section. The train will accelerate with full power to the upper bound V_coh or speed limit V_lmt (depending on which one

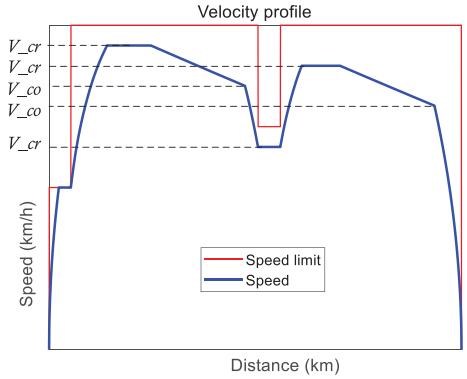

FIGURE 3 CC speed profiles. CC, cruising–coasting.

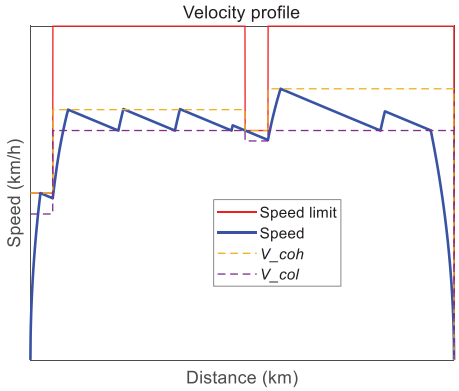

FIGURE 4 CR speed profiles. CR, coasting–remotoring.

is lower) and then coast to the lower bound V_col. This process repeats until the brake caused by the final stop or speed limit decreases. The speed profiles of the CR strategy are shown in Figure 4. In this schematic, the dashed yellow line and purple lines present the upper and lower bound speeds. Since the control speed pairs are independent for different speed limit sections, the values of yellow line in different speed limit sections can be different. Although the values of the purple line in the second and fourth speed limit sections are the same, they differ from those of the other speed limit sections. Note that if the upper and lower bounds are equal or the lower bound is not smaller than the speed limit, the train will cruise at the equal speed or the speed limit.

3 | TRAIN DRIVING ENERGY DISTRIBUTION ANALYSIS

3.1 | Traction energy distribution

To study the energy consumption of CC and CR, the Energy Conservation Law is introduced. Figure 5 shows the energy conversion of a train. Mechanical traction energy will be used to accelerate the train, work against resistance (motion loss) and gravity, as well as consumed by braking (braking loss).

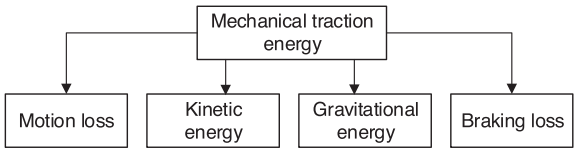

FIGURE 5 Energy conversion diagram.

When the train moves from one random distance index s to another random distance index e, the generic energy distribution can be expressed as Equation (5).

$$E_t(s,e) = E_r(s,e) + E_k(s,e) + E_g(s,e) + E_b(s,e) \quad (5)$$

$E_t(s,e)$ is the mechanical traction energy from s to e, which can be expressed as Equation (6). $E_r(s,e)$ is the motion loss as Equation (7). $E_k(s,e)$ is the change of kinetic energy expressed by Equation (8). $E_g(s,e)$ is the change of gravitational energy as shown in Equation (9). $E_b(s,e)$ is the braking loss as shown in Equation (10).

$$E_t(s,e) = \sum_{i=s}^{e} F_t(i)\,\Delta s \quad (6)$$

$$E_r(s,e) = \sum_{i=s}^{e} R(i)\,\Delta s \quad (7)$$

$$E_k(s,e) = \frac{1}{2}Mv(e)^2 - \frac{1}{2}Mv(s)^2 \quad (8)$$

$$E_g(s,e) = Mgh(e) - Mgh(s) \quad (9)$$

$$E_b(s,e) = \sum_{i=s}^{e} F_b(i)\,\Delta s \quad (10)$$

In the equations above, Δs is the distance interval, M is the mass of the train, g is the acceleration due to gravity, $h(s)$ and $h(e)$ are the altitudes at s and e, $v(s)$ and $v(e)$ are the speed at s and e. $F_t(i)$ and $F_b(i)$ are the tractive and braking efforts, respectively.

3.2 | Comparison section selecting

To compare the different driving strategies for the CC and CR with the same journey time, we will select the section to be compared in this part. For each CC speed profile, we can find a CR speed profile with the same braking start speed, which is illustrated in Figure 6. In this figure, three pairs of CC and CR speed profiles, each pair with the same running time, are shown. Despite the overlaps, the start point of our research is s, and the endpoint is e as shown in Figure 6. The following analysis is based on the assumption that the difference between the speed limit and the cruising speed is big enough to realise the coasting–remotoring.

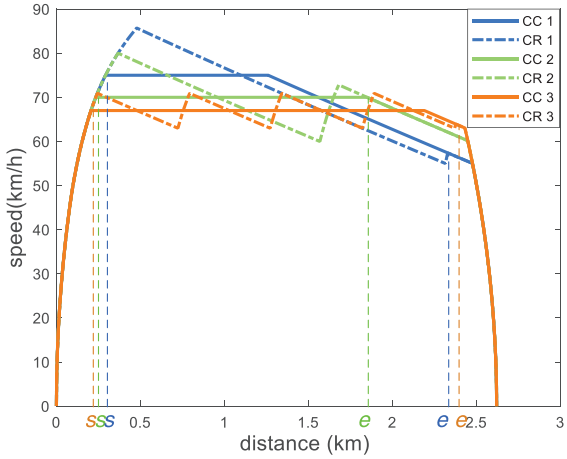

FIGURE 6 Speed profile schematic of CC and CR. CC, cruising–coasting; CR, coasting–remotoring.

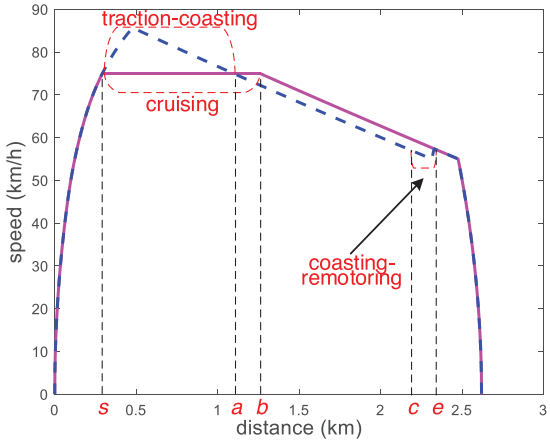

FIGURE 7 Simplifying the comparison between CC and CR. CC, cruising–coasting; CR, coasting–remotoring.

3.3 | The influence of different gradients on energy distribution

3.3.1 | Gradient classification

The gradient can be divided into five types: level, steep uphill, steep downhill, gentle uphill, and gentle downhill. The steep uphill section is where the train has insufficient power to maintain a cruising speed. The steep downhill section is where the train accelerates while coasting [1, 38]. The gentle hill sections include uphill and downhill sections except the steep ones.

3.3.2 | Speed profiles of the two strategies on different gradients

From Figure 6, we can see the difference between CC and CR focuses on cruising–coasting and coasting–remotoring, which start from s and end at e. For each type of gradient over s to e, the coasting of CC from b to e is identical as the coasting of CR from a to c, as illustrated in Figure 7. Therefore, comparison between CC and CR can be transferred into comparing cruising of CC (from s to b) and coasting–remotoring of CR (from s to a and c to e). The remaining coasting–remotoring could be within a single interval as CR2 in Figure 6, or divided into two non-contiguous intervals (s to a and c to e) as CR1 and CR3.

3.3.3 | Energy consumption comparison on non-steep track

For non-steep tracks, from point s to e of Figure 7, the changes in gravitational energy and kinetic energy of the two speed profiles are identical. According to Equation (5), the difference in the traction energy consumption only relates to the motion loss. Assume the journey time of CC from s to b is t_{sb}, we have

$$t_{sb} = t_{sa} + t_{ce} \tag{11}$$

where t_{sa} and t_{ce} are the journey times of CR from s to a and c to e. After eliminating the identical coasting part (b to e of CC and a to c of CR), we assume the time index at the start point of comparison is k and the end point as j with the time interval Δt. According to Equations (3) and (7), the motion loss of cruising regime($E_{r\_cr}(k,j)$) and coating–remotoring regime ($E_{r\_csm}(k,j)$) can be expressed as Equations (12) and (13).

$$E_{r\_cr}(k,j) = A\Delta t \sum_{i=k}^{j} \bar{v} + B\Delta t \sum_{i=k}^{j} \bar{v}^2 + C\Delta t \sum_{i=k}^{j} \bar{v}^3 \tag{12}$$

$$E_{r\_csm}(k,j) = A\Delta t \sum_{i=k}^{j} v(i) + B\Delta t \sum_{i=k}^{j} v(i)^2 + C\Delta t \sum_{i=k}^{j} v(i)^3 \tag{13}$$

where $\bar{v}$ is the cruising speed, as well as the average speed of coasting–remotoring. Since the displacements from k to j are the same, $\Delta t \sum_{i=k}^{j} \bar{v}$ in Equation (12) is equal to $\Delta t \sum_{i=k}^{j} v(i)$ in Equation (13). According to the Cauchy–Bunyakovsky–Schwarz inequality and the generalised Hölder's inequality [39], we have Equations (14) and (15).

$$\sum_{i=k}^{j} \bar{v}^2 = \frac{1}{(j-k+1)} \left(\sum_{i=k}^{j} v(i) \right)^2 \le \sum_{i=k}^{j} v(i)^2 \tag{14}$$

$$\sum_{i=k}^{j} \bar{v}^3 = \frac{1}{(j-k+1)^2} \left(\sum_{i=k}^{j} v(i) \right)^3 \le \sum_{i=k}^{j} v(i)^3 \tag{15}$$

According to Equations (12) to (15), $E_{r\_cr}(k,j) \le E_{\mathrm{r\_csm}}(k,j)$. $E_{r_cr}(k,j)$is equal to $E_{r\_csm}(k,j)$ only when all the $v(i)$ are equal to $\bar{v}$. Therefore, for the level, gentle uphill and gentle downhill, we have $E_{t\_cr}(s,e) \le E_{t\_csm}(s,e)$, which means that the traction energy consumption of cruising is always smaller than or equal to that of coasting–remotoring.

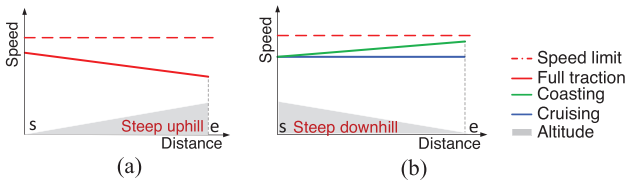

FIGURE 8 Cruising and coasting–remotoring speed profiles on steep track. (a) Steep uphill, (b) steep downhill.

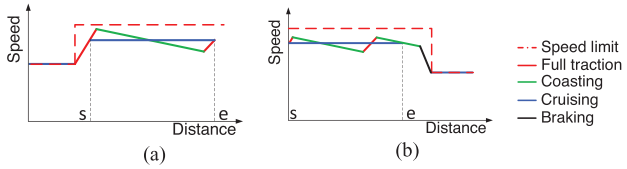

FIGURE 9 Schematic diagram of cruising and coasting–remotoring speed profiles when the speed limit changes. (a) Speed limit increase, (b) speed limit decrease.

3.3.4 | Performance comparison on the steep track

For the steep uphill section, as shown in Figure 8a, even when full power traction is applied, the speed will also decrease. As a result, if the cruising regime is used, the train will be using full power traction, and its speed will decrease. If the start and end speeds of the coasting–remotoring regime are both equal to the cruising regime, full traction power must be applied throughout this section. So, the two control regimes perform identically for this type of gradient.

On the steep downhill, to maintain cruising, braking must be applied. The speed profile is presented in Figure 8b. The speed will increase in the coasting–remotoring regime even when coasting is applied. Therefore, the final speed will be greater than the cruising speed. Although neither regime requires any power, the coasting–remotoring regime has a shorter running time and higher final kinetic energy.

Above all, only when there is a steep downhill during the trip can CR be more energy-efficient than CC.

3.3.5 | The influence of different speed limits on energy distribution

To study the influence of speed limit, we assume that the gradient is zero. When the speed limit changes, both the cruising regime and the coasting–remotoring regime will be interrupted. The reactions of CC and CR are illustrated in Figure 9.

When the speed limit increases, there is a chance that the cruising speed or the upper and lower bounds will not change. But if these control speeds increase, the full power traction regime will be implemented, as shown in Figure 9a. Similarly, if the control speeds decrease with the decrease in the speed limit, the speed profiles of CC and CR will be like Figure 9b. It can be seen from Figures 9a and 9b that the change in speed limit will transfer the problem into comparing CC and CR in

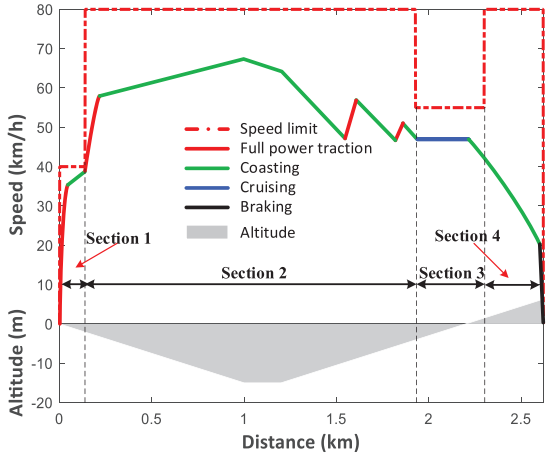

FIGURE 10 Example of region division and control regimes.

several subsections on a level track. According to the analysis results of Section 3.3, the energy consumption of the cruising regime is equal to or smaller than coasting–remotoring. Therefore, changing the speed limit can only make CC and CR more flexible since the control speeds will change in different speed limit sections, but it will not make CR outperform CC.

4 | IMPROVED ENERGY-EFFICIENT DRIVING STRATEGY

From the analysis above, the optimal driving strategy is related to the gradients and speed limits of the route. In this section, we propose an improved energy-efficient train driving strategy as shown in Figure 10. First, to simplify the driving strategy, the route is divided into subsections according to the speed limits, which means that there might be more than one gradient in a substation. The control strategy and number of decision variables for each subsection will then be determined by the gradients and the analysis results in Section 3. If CC is applied in a subsection, the decision variables will be cruising speed and the switching speed from coasting to braking. For the CR strategy, one upper bound and two lower bounds will be the decision variables. In the case of the coasting before cruising strategy, the decision variable will involve the switching speed from full power traction to coasting. Finally, these decision variables will be optimised using the NSGA-II algorithm, with the objectives of minimising running time and energy consumption.

4.1 | Identify the control strategies and decision variables

There are various methods for segmenting a route into subsections. These include dividing based on fixed intervals [40], treating areas with uniform slopes or consistent speed limits as separate subsections [41, 42], or a combination of speed limits with fixed intervals [43]. However, these methods result in a high number of subsections, which makes it challenging to pinpoint the optimal solution. In line with the analysis in Section

TABLE 1 Combination of speed limits and steep downhills.

$(\bar{V}\_s < G\_s)$ && $(G\_e < \bar{V}\_e)$	$(\bar{V}\_s \geq G\_s)$ && $(\bar{V}\_s < G\_e < \bar{V}\_e)$	$(\bar{V}\_s < G\_s < \bar{V}\_e)$ && $(G\_e \leq \bar{V}\_e)$	$(\bar{V}\_s > G\_s)$ && $(G\_e > \bar{V}\_e)$
(a)	(b)	(c)	(d)
(e)	(f)	(g)	(h)

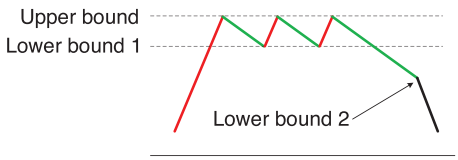

FIGURE 11 Proposed speed profile for situation (a) to (c) and (e) to (g).

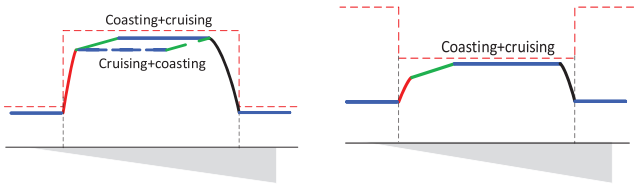

FIGURE 12 Speed limit covered by one steep downhill section.

3 of this study, we divide the subsections based on speed limits, considering the impact of gradients by examining the interplay between gradient and speed limits.

According to the definition of the steep downhill, the minimum value of steep downhill is calculated using the following equation:

$$stp\_g = \left(A + Bv + Cv^2\right)/Mg \tag{16}$$

If the absolute value of downhill is higher than stp_g, it is recognised as a steep downhill. Based on the analysis in Section 3.3, for routes without steep downhill, CR cannot outperform CC. Therefore, in the subsection without steep downhill, CC will be applied. In contrast, if the steep downhill overlaps with the subsection, there will be eight different situations, as presented in Table 1. Assume the start and end positions of the speed limit section and gradient section are $\bar{V}\_s$, $\bar{V}\_e$, G_s, and G_e, respectively. The eight situations can be expressed by four sets of inequations as shown in this table. Situations (a) to (c) and (e) to (g) show the subsections that include not only steep downhill. These situations can combine with each other. While (d) and (h) illustrate the subsections covered by the steep downhills. For (a) to (c) and (e) to (g) or combinations of them, coasting–remotoring can be more energy efficient than cruising (analysis result of Section 3.3). Therefore, we set one pair of upper and lower bounds for the coasting–remotoring regime to use the steep downhill fully. To make full use of the final coasting, another coasting control speed is set, as shown in Figure 11. In other words, for situations other than (d) and (h), three control variables, one upper bound and two lower bounds, are set up.

For situations (d) and (h), if coasting is needed to consume the surplus time, the coasting regime must be before cruising. Referring to Figure 12a, the solid green and blue lines illustrate when coasting is applied first. The dashed lines represent the situation when cruising is applied first. The average speed of the solid lines is higher than the dashed lines. However, the energy consumption corresponding to these two strategies is identical since energy is consumed only in the traction regime. Even though coasting is mostly not needed in the subsection, as shown in Figure 12b, once coasting is required, it must be applied before cruising to improve energy efficiency. Therefore, for the subsection covered by a steep downhill section, only one decision variable is needed, which is the speed of the coasting start point. For all combinations of the speed limits and gradients, the procedure to identify the control strategies and decision variables is illustrated in Figure 13.

4.2 | Pareto frontier calculation with NSGA-II

The new energy-efficient speed profile is constructed by a set of optimal control speeds. By considering the energy consumption and running time as two objectives, we formulate the optimal driving problem as a multi-objective model, which is given as

$$\begin{aligned} &min \sum_{i=1}^{N} E_t(i) \\ &min \sum_{i=1}^{N} T(i) \\ &s.t. \begin{cases} v(0) = 0,\ v(N) = 0 \\ s(0) = 0,\ s(N) = S \\ v(i) \leq V\_lmt(i)/3.6 \\ V\_ctl(p,q) \leq V\_lmt(p) \\ -A_{max} \leq a(i) \leq A_{max} \end{cases} \end{aligned} \tag{17}$$

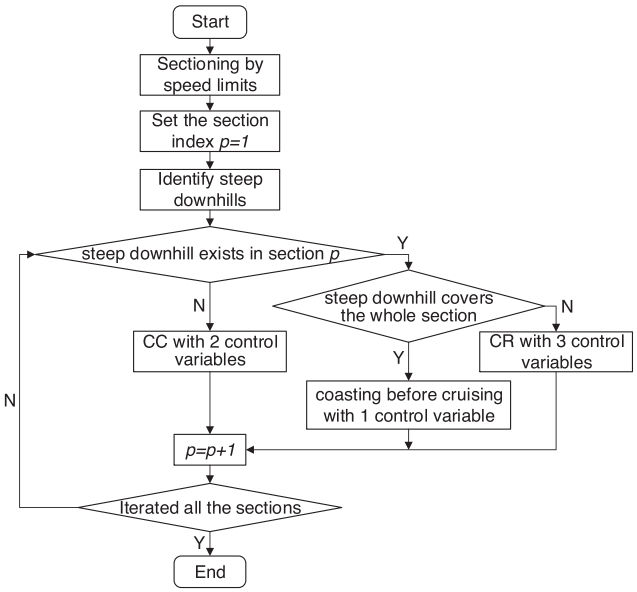

FIGURE 13 Control strategies and decision variables identification.

where N is the number of distance intervals in an interstation, $T(i)$ is the running time for every interval, S is the length of the interstation, $V\_ctl(p, q)$ is the qth control speed of the pth subsection, $V\_lmt(p)$ is the speed restriction value of the pth subsection.

The optimisation method with NSGA-II can be summarised as follows:

- Step 1: Determine the number of control speeds for every subsection according to the method in Section 3.1. Use K to represent the total number of control speeds, which are also decision variables.
- Step 2: Define K genes in each chromosome based on K control speeds. Generate the random population.
- Step 3: Calculate the fitness values for every individual, specifically the energy consumption and running time.
- Step 4: Sort the individuals with their non-dominated level (non-dominated individuals as the first level, the other non-dominated individuals in the subset as the second level, and so on, until all the individuals are ranked).
- Step 5: Select parents according to the non-dominated level.
- Step 6: Crossover and mutation. Select two individuals randomly from the parents. Apply polynomial crossing in this algorithm. At the same time, make sure the genes are under the constraints after crossover. Then, choose the chromosomes to be mutated randomly. The value of these chromosomes after mutation is also random. Namely, the control speeds are modified for arbitrary values under constraint conditions.
- Step 7: Combine the initial population and the children. Sort these individuals and select the population for the next generation.
- Step 8: Return Step 2 if the iterations have not been completed.

TABLE 2 Parameters of the rolling stock.

Parameters	Value of the rolling stock
Static train mass [tonnes]	175.6
Rotary allowance	0.07
Train resistance [N, N/(m/s), N/(m^2/s^2)]	[3.856, 0.267, 0.020]
Maximum traction power [kW]	2387
Maximum braking power [kW]	2377
Maximum operation speed [km/h]	80
Maximum tractive effort [kN]	191.7
Maximum braking effort [kN]	142.6

TABLE 3 Gradient data and speed limits.

Segments (km)	Gradients (‰)	Segments (km)	Speed limits (km/h)
0–1.00	−15	0–0.14	40
1.00–1.20	0	0.14–1.93	80
1.20–2.62	15	1.93–2.30	55
–	–	2.30–2.62	80

5 | CASE STUDY

To illustrate the effectiveness of CC_CR and investigate the performance of CC and CR, three simulators based on these driving strategies are applied to four scenarios using MATLAB R2021a on a PC with 2.30 GHz Intel i7-11800H CPU and 16GB RAM. The crossover and mutation rates of NSGA-II are 0.8 and 0.1, respectively. Each optimization process involves 200 individuals and 300 iterations.

5.1 | Simulation parameters

A typical metro rolling stock is used in the case study. Its parameters are shown in Table 2. Practical gradients and speed limits are shown in Table 3. The positive gradient value represents the uphill, and the negative value is for the downhill. According to the definition of steep downhill, the route between 0 and 1.2 km is recognised as a steep downhill section for the rolling stock. To investigate the performance of CC, CR, and CC_CR on different routes, we distinguish the four scenarios using gradient and speed limit data, which is listed below.

- Scenario 1: all gradients are zero; all speed limits are 80 km/h.
- Scenario 2: all gradients are zero; the speed limit changes according to Table 3.
- Scenario 3: the gradient changes according to Table 3; all speed limits are 80 km/h.
- Scenario 4: both gradient and speed limit change according to Table 3.

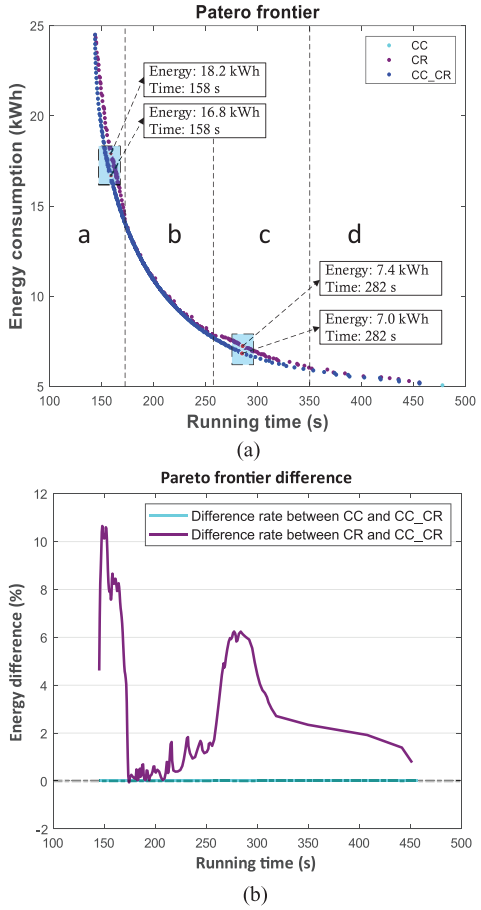

FIGURE 14 Pareto frontiers and their differences in scenario 1. (a) Pareto frontiers in scenario 1. (b) The difference between these Pareto frontiers.

5.2 | Simulation results

Since there is a trade-off between running time and energy consumption, the simulation results are expressed as Pareto frontiers of these two indexes. The Pareto frontiers and their energy consumption difference rates of CC, CR, and CC_CR in these four scenarios are presented in the following sections.

5.2.1 | Results of scenario 1

Since there is no steep downhill in scenario 1, CC_CR will use the same strategy as CC. Figure 14 shows the Pareto frontiers of CC, CR, and CC_CR. The Pareto frontier of CC overlaps with CC_CR in Figure 14a, and the difference rate between CC and CC_CR is zero in Figure 14b, which indicates that CC and CC_CR are the same in this scenario. In Figure 14a, the Pareto frontiers are divided into four sections. The optimal energy consumption of CC and CR in Section 'b' and Section 'd' are almost the same. That is because, in Section 'b', acceleration, coasting, and final braking are all possible options for CC and CR's best control modes. So, the energy consumption of the two strategies can be the same. While, for Section 'd', extending the scheduled time leads to a reduction in total energy consumption.

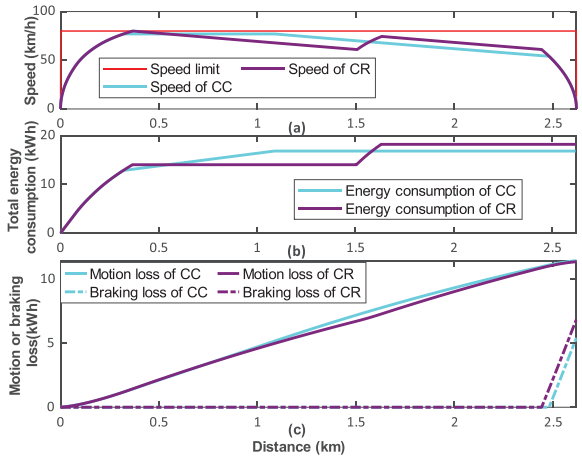

FIGURE 15 CC and CR when the running time is 158 s. CC, cruising–coasting; CR, coasting–remotoring.

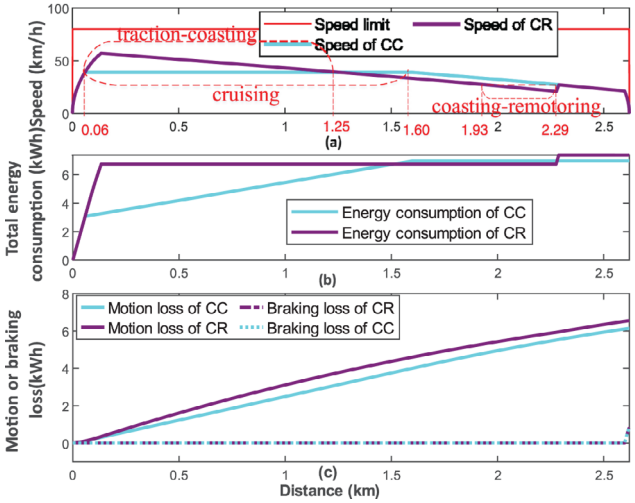

FIGURE 16 CC and CR when the running time is 282 s. CC, cruising–coasting; CR, coasting–remotoring.

Therefore, their difference can be neglected. In contrast, the difference rates between CC and CR in Section 'a' and 'c' can reach 11% and 6% (Figure 14b), respectively.

To analyse the reason why CC consumes less energy than CR, the speed and energy consumption profiles corresponding to two pairs of points, two in Section 'a' and one in Section 'c', are illustrated in Figures 15 to 16. No matter which control strategy is applied, the kinetic energy changes of the whole journey are zero, and the gravitational energy changes are the same. Therefore, according to Equation (5), the energy consumption difference between different driving strategies is only related to the motion loss and braking loss. As a result, the motion loss and braking loss are also presented in the figures. Their control speeds, energy consumption, and running time are presented in Table 4.

Figure 15 shows the results when the running time is 158 s. Here the cruising speed of CC is lower than the speed limit. However, the difference between cruising speed and coasting

TABLE 4 Comparison of CC and CR in Section 'a' and Section 'c', scenario 1.

Pareto points	Driving strategy	Control speed 1 (km/h)	Control speed 2 (km/h)	Energy consumption (kWh)	Running time (s)
Pair 1	CC	77 (cruising speed)	54 (coasting speed)	16.8	158
	CR	80 (upper bound)	61 (lower bound)	18.2	158
Pair 2	CC	39 (cruising speed)	21 (coasting speed)	7.0	282
	CR	57 (upper bound)	21 (lower bound)	7.4	282

CC, cruising–coasting; CR, coasting–remotoring.

speed is 23 km/h, much higher than the difference between cruising speed and the speed limit, which is 3 km/h. If CR approximates the cruising speed of CC, it will start coasting at a very high speed, which means that the running time is shorter and the energy consumption is higher. While if CR coasts as CC, in the end, its average speed will be much lower. So, the speed profile of CC in Figure 15a is a compromise between these two assumptions. Therefore, it is also because of the higher final coasting speed that the energy consumption of CR is higher.

Different from the points in Section 'a', in Section 'c', when CC is applied, there will be a cruising mode at a speed much lower than the speed limit and then coasting before braking. For example, when the running time is 282 s. From Figure 16a, we can see CC and CR start braking at the same speed. Therefore, the braking loss of these two strategies overlaps. Since the braking regime is only applied before the end of the journey and the braking start speed is 21 km/h, which is very low, there is only a small increase in braking loss, as indicated in Figure 16c.

The difference between these two speed profiles is the cruising section (0.058–1.600 km) of CC and motoring–coasting (0.058–1.245 km) and coasting–remotoring (1.934–2.289 km) of CR as illustrated in Figure 16a. According to the analysis of Section 3.3, the motion loss of CR is higher than CC, which is demonstrated in Figure 16c. Therefore, in Section 'c', the higher energy consumption of CR is caused by the motion loss.

5.2.2 | Results of scenario 2

In scenario 2, the influence of speed limits is added to the route. The Pareto frontiers of these three strategies are presented in Figure 17a. Within our expectation, CC almost overlaps CC_CR, because when there is no steep downhill in the route, the control strategy of CC_CR should be the same as CC. Since the Pareto frontiers are obtained from NSGA-II, there is a slight variation between them, which can be seen in Figure 17b. While the energy efficiency of CR is lower than CC and CC_CR in Section 'a'. This is caused by the same reasons as in Section 'a' of scenario 1. According to the analysis in Section 3.4, the speed limit data can increase the flexibility of these three strategies by dividing the route into different control sections. Therefore, the length of the speed deviation section between coasting–remotoring and cruising, as shown in Figure 16a, can be reduced. As a result, the difference between CC and CR in Section 'c' of scenario 1 cannot be seen in this scenario.

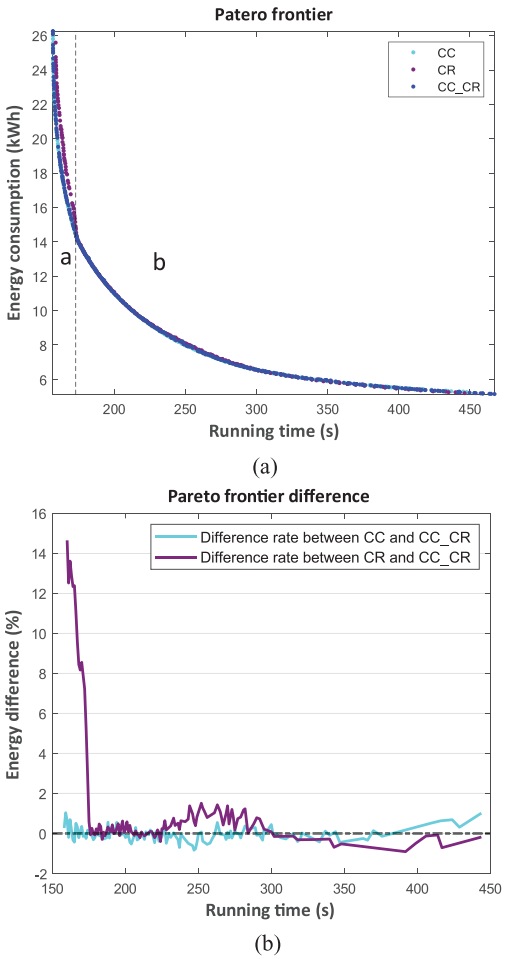

FIGURE 17 Pareto frontiers and their differences in scenario 2. (a) Pareto frontiers in scenario 2. (b) The difference between these Pareto frontiers.

5.2.3 | Results of scenario 3

In scenario 3, the influence of gradient is added. As we can see from Figure 18a, the energy efficiency of CC is similar to CC_CR, both better than CR in Section 'a'. The difference rate between CR and CC_CR can reach up to 12% (Figure 18b), similar to scenarios 1 and 2. While different from the scenarios above, the energy efficiency of CC decreases from Section 'b'. To analyse the cause of the change in CC and compare these three strategies, two sets of points in Section 'b' and Section 'c' of Figure 18a are chosen. Their control variables,

TABLE 5 Comparison of CC, CR and CC_CR in Section 'b' and Section 'c', scenario 3.

Pareto points	Driving strategy	Control speed 1 (km/h)	Control speed 2 (km/h)	Control speed 3 (km/h)	Energy consumption (kWh)	Running time (s)
Set 1	CC	80 (cruising speed)	33 (coasting speed)	–	17.7	157
	CR	76 (upper bound)	51 (lower bound)	–	18.6	157
	CC_CR	75 (upper bound)	69 (lower bound 1)	39 (lower bound 2)	17.0	157
Set 2	CC	50 (cruising)	20 (coasting)	–	15.2	201
	CR	61 (higher bound)	24 (lower bound)	–	12.9	201
	CC_CR	52 (higher bound)	46 (lower bound 1)	20 (lower bound 2)	12.2	201

CC, cruising–coasting; CR, coasting–remotoring.

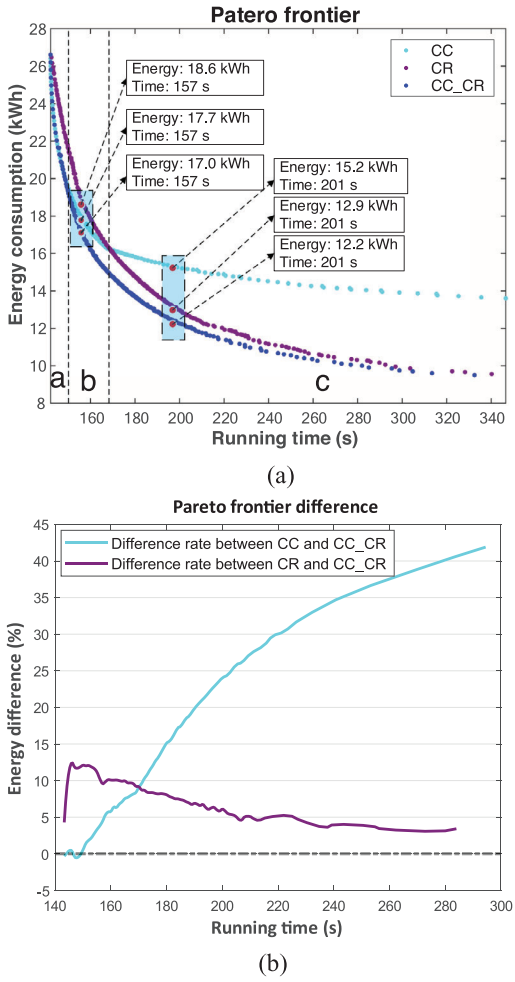

FIGURE 18 Pareto frontiers and their differences in scenario 3. (a) Pareto frontiers in scenario 3, (b) the difference between these Pareto frontiers.

energy consumption, and running times are presented in Table 5.

The motion and energy consumption characteristics corresponding to three points in Section 'b' with the same running time 157 s are illustrated in Figure 19. From Figure 19c, we can see the cruising of CC at the steep downhill leads to about 1 kWh braking loss. In contrast, CR and CC_CR can use the energy of the steep downhill by coasting. Therefore,

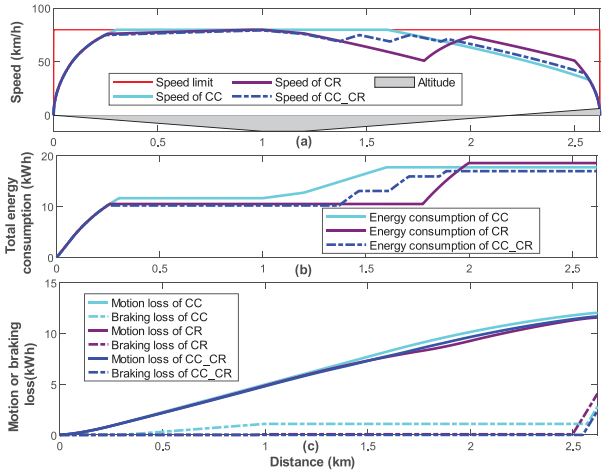

FIGURE 19 CC, CR, and CC_CR when the running time is 157 s. CC, cruising–coasting; CR, coasting–remotoring.

when steep downhill appears during the cruising regime, CC will lose its advantage in energy consumption. For CR, the reason for higher energy consumption is still the last braking loss, just as in Section 'a'. In Section 'c' of the Pareto frontiers, the energy consumptions of CC_CR and CR are lower than CC.

The profiles of these three strategies with a running time of 201 s are presented in Figure 20. From Figure 20c, the braking loss profile of CR overlaps CC_CR. In contrast, the CC's braking loss grows rapidly during cruising on the steep downhill, which leads to a difference of 3.5 kWh between CC and the other two strategies. Although the motion loss of CC is the lowest, the difference between them is slight, only 1.2 and 0.8 kWh lower than CR and CC_CR, respectively. Overall, the advantage of CR and CC_CR is mainly due to coasting on the steep downhill. The performance of CC_CR is the best, regardless of the value of the proposed running time.

5.2.4 | Results of scenario 4

In the fourth scenario, the gradient and speed limit data are both added to the route. The route is divided into four subsections by the speed limits, which increases the flexibility of

TABLE 6 Comparison of CC, CR, and CC_CR when the running time is 209 s, scenario 4.

Driving strategy	Control speed of Section 1 (km/h)		Control speed of Section 2 (km/h)			Control speed of Section 3 (km/h)		Control speed of Section 4 (km/h)		Energy consumption (kWh)	Running time (s)
CC	37	36	76	28		33	24	59	20	13.1	209
CR	33	21	49	47		53	42	24	20	11.8	209
CC_CR	35		49	47	58	47	35	42	20	11.8	209

CC, cruising–coasting; CR, coasting–remotoring.

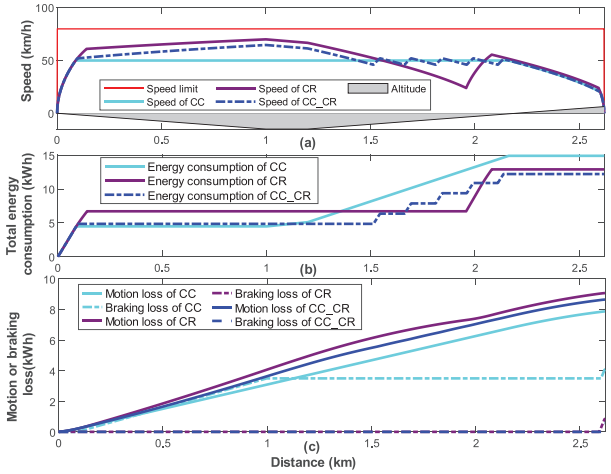

FIGURE 20 CC, CR, and CC_CR when the running time is 201 s. CC, cruising–coasting; CR, coasting–remotoring.

these three strategies. Compared with scenario 3, the difference between them has decreased. CR and CC_CR are almost the same, especially when the proposed running time is longer than 195 s, which can be seen in Figures 21a and 21b. When the run time exceeds 250 s, the energy and time consumption of CC increases, so these points should not be on the Pareto front. However, we still show these points here to compare CC's energy consumption with the other two strategies. The difference between CC and CC_CR is similar to that of scenario three, except when the running time is between 180 and 250 s. In this time range, take the running time 209 s as an example (Figure 22).

The control variables of these three strategies are shown in Table 6. The numbers of control variables of CC_CR for the four subsections are 1, 3, 2, and 2, respectively. We can see from Figure 22 that the higher energy consumption of CC is mainly because of the braking loss in the first subsection and the motion loss in the second subsection. Since the flexibility of CC has been increased, the braking loss caused by cruising in the second subsection, which is the main reason for high energy consumption in scenario 3 has been eliminated. When the running time is less than 180 s, CC must cruise at high speed. Similar to scenario 3, the energy of steep downhill is wasted. After 250 s, CC has to maintain a low speed that cannot be affected by the speed limit. Therefore, in this time range, the difference between CC and CC_CR is similar to scenario 3.

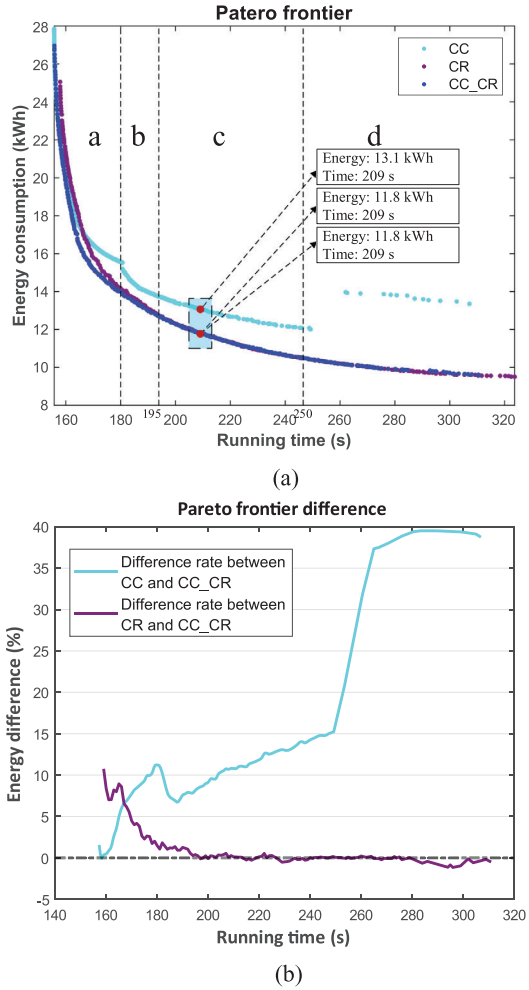

FIGURE 21 Pareto frontiers and their differences in scenario 4. (a) Pareto frontiers in scenario 4, (b) the difference between these Pareto frontiers.

5.2.5 | Verification with real metro line

In this part, Guangzhou metro line 7 is introduced to verify the effectiveness of the proposed strategy, CC_CR. The route data and scheduled time can refer to [14]. The optimisation results obtained by CC, CR, and CC_CR are presented in Table 7. The optimal speed profiles are illustrated in Figure 23. IS1-8 represent the eight inter-stations. The steep downhill exists in IS 2, 4, 5, 6, and 8. Therefore, in IS 1, 3, and 7, where no steep downhill exists, the optimisation results of CC and CC_CR are similar. Their speed profiles almost overlap. In IS 2 and 5, CC_CR can

TABLE 7 Scheduled timetable and the optimisation results.

Inter-station	Scheduled journey time [s]	Optimal with CC		Optimal with CR		Optimal with CC_CR	
		Time [s]	Energy [kWh]	Time [s]	Energy [kWh]	Time [s]	Energy [kWh]
IS 1	130	129	9.15	129	9.31	129	9.15
IS 2	170	170	21.90	170	20.75	169	20.07
IS 3	185	185	25.41	185	26.34	184	25.40
IS 4	180	180	17.70	181	17.17	177	17.00
IS 5	185	185	23.68	185	24.08	185	23.04
IS 6	220	220	17.90	220	18.21	219	17.63
IS 7	210	211	23.19	211	24.20	214	23.05
IS 8	330	328	42.07	327	43.21	329	41.91

CC, cruising–coasting; CR, coasting–remotoring.

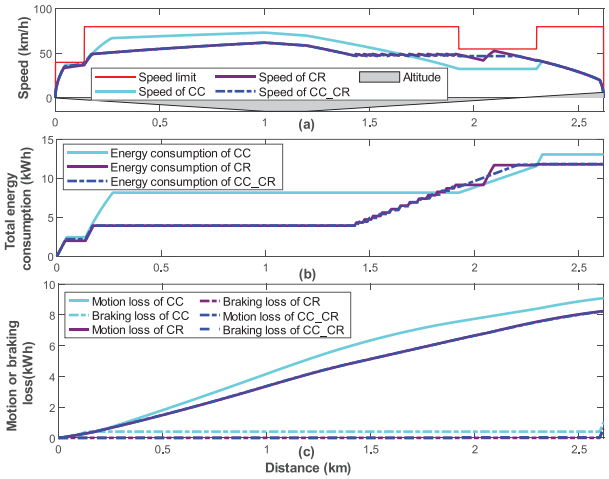

FIGURE 22 CC, CR, and CC_CR when the running time is 209 s. CC, cruising–coasting; CR, coasting–remotoring.

use more coasting to save energy. In contrast, CC can only use partial braking to keep the cruising speed. Although CC can also coast on the steep downhill sections in IS 4, 6, and 8 because of the multiple control speed sets for different speed limit sections, the gravitational energy may not be fully used especially in IS 4.

Figure 24 presents the energy consumption difference rates between CC and CC_CR, as well as CR and CC_CR for each inter-station. 'CC vs CC_CR' and 'CR vs CC_CR' means the

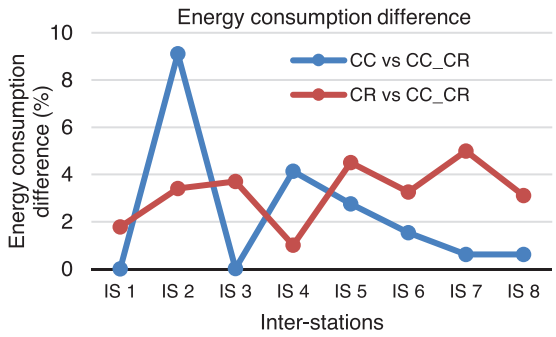

FIGURE 24 Energy consumption difference of the three strategies.

energy consumption of CC or CR minus CC_CR and then divided by CC_CR. From this figure, we can see in IS 2 and 4, CC consumes more energy than CR and CC_CR. The difference rate between CC and CC_CR can reach about 9%. In other inter-stations, CR consumes more energy than CC and CC_CR. The maximum difference rate between CR and CC_CR is 5%. Although steep downhill also exists in IS 5, 6, and 8, the energy consumption of CR is higher than CR. This is still consistent with the analysis results in Section 3.3 and also illustrates the necessity of adding another coasting control speed to traditional CR as shown in Figure 11. Finally, we can also see that these difference rates are all positive, which means CC_CR can achieve the lowest energy consumption in all inter-stations.

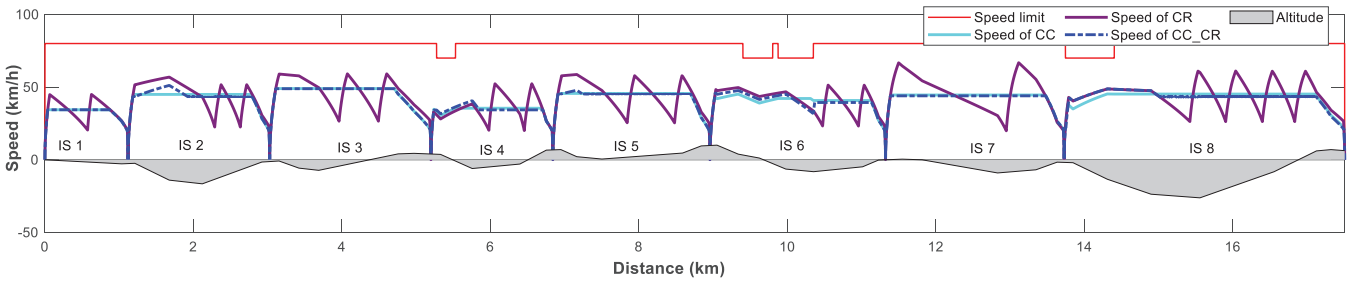

FIGURE 23 The optimal speed profile by CC, CR, and CC_CR. CC, cruising–coasting; CR, coasting–remotoring.

Therefore, the effectiveness of the proposed strategy is further verified.

6 | CONCLUSION

This paper analysed the performance of two typical energy-efficient driving strategies CC and CR, and then developed a new energy-efficient driving strategy, CC_CR based on the analysis results. The theoretical investigation of how gradients and speed limitations affect CC and CR gives two findings. First, only when steep downhill exists can CR consume less energy than CC. The other one is that speed limits can improve the flexibility of these two strategies but cannot eliminate the advantage of CC. Based on these two findings, the optimal driving strategy is developed. Simulation results with four scenarios demonstrated the effectiveness of CC_CR in energy saving. The Pareto frontiers of CC, CR, and CC_CR show that CC always performs equally or better than CR, if the route does not have a steep downhill, regardless of whether the speed limit changes or not. On routes with steep downhill, the energy efficiency of CR will be higher than that of CC, when the suggested travel time is slack. In comparison, CC_CR is always the best strategy. The energy consumption can reduce by up to 15% and 42%, respectively, compared to CR and CC. The case study with Guangzhou metro line 7 was also carried out, which further verified the effectiveness of the proposed strategy.

NOMENCLATURE

Δs	distance interval for discretisation [m]
a	acceleration of the vehicle [m/s^2]
v	speed of the vehicle [m/s]
s	vehicle position along the track [m]
F	tractive or braking effort [N]
R	vehicle resistance [N]
G	gravity effort in the direction of train motion [N]
M	mass of the vehicle [kg]
λ	rotary allowance
A	Davis equation constant [N]
B	Davis equation linear term constant [N/(m/s)]
C	Davis equation quadratic term constant [N/(m/s)^2]
g	acceleration due to gravity [m/s^2]
$grad$	gradient of the route [‰]
E_t	mechanical traction energy [kWh]
E_r	motion loss [kWh]
E_k	change of kinetic energy [kWh]
E_g	change of gravitational energy [kWh]
E_b	braking loss [kWh]
h	altitude [m]
F_t	tractive effort [N]
F_b	braking effort [N]
$\bar{v}$	average speed [m/s]
Δt	time interval [s]
E_{r_cr}	motion loss of cruising [kWh]
E_{r_csm}	motion loss of coasting-remotoring [kWh]
E_{t_cr}	traction energy used by cruising [kWh]
E_{t_cr}	traction energy used by coasting-remotoring [kWh]
T	journey time [s]
N	number of distance intervals
S	total length of one interstation [m]
V_lmt	train maximum speed due to speed limit [km/h]
V_ctl	driving control speed [km/h]
K	number of control speeds
V_cr	cruising speed [km/h]
V_co	coasting speed [km/h]
V_coh	upper bound of coasting-remotoring [km/h]
V_col	lower bound of coasting-remotoring [km/h]
stp_g	minimum gradient value of the steep downhill
$\bar{V}\_s$	start position of a speed limit section[km]
$\bar{V}\_e$	end position of a speed limit section[km]
G_s	start position of a constant gradient section[km]
G_e	end position of a constant gradient section[km]

AUTHOR CONTRIBUTIONS

Xiao Liu: Conceptualization; investigation; methodology; software; writing—original draft; writing—review & editing. **Zhongbei Tian**: Conceptualization; methodology; supervision; writing—review & editing. **Lin Jiang**: Conceptualization; supervision. **Shaofeng Lu**: Conceptualization; supervision. **Pingliang Zeng**: Conceptualization; supervision.

CONFLICT OF INTEREST STATEMENT

The authors declare no conflict of interest.

DATA AVAILABILITY STATEMENT

Data sharing not applicable to this article as no datasets were generated or analysed during the current study.

ORCID

Zhongbei Tian https://orcid.org/0009-0009-5629-4072
Lin Jiang https://orcid.org/0000-0001-6531-2791

REFERENCES

1. Scheepmaker, G. M., Goverde, R. M. P., Kroon, L. G.: Review of energy-efficient train control and timetabling. Eur. J. Oper. Res. 257(2), 355–376 (2017)
2. Lu, S., Hillmansen, S., Ho, T. K., Roberts, C.: Single-train trajectory optimization. IEEE Trans. Intell. Transp. Syst. 14(2), 743–750 (2013)
3. Lu, S., Wang, M. Q., Weston, P., Chen, S., Yang, J.: Partial train speed trajectory optimization using mixed-integer linear programming. IEEE Trans. Intell. Transp. Syst. 17(10), 2911–2920 (2016)
4. Cao, Y., Zhang, Z., Cheng, F., Su, S.: Trajectory optimization for high-speed trains via a mixed integer linear programming approach. IEEE Trans. Intell. Transp. Syst. 23(10), 17666–17676 (2022)
5. Wang, Y., De Schutter, B., van den Boom, T. J. J., Ning, B.: Optimal trajectory planning for trains – A pseudospectral method and a mixed integer linear programming approach. Transp. Res. C Emerg. Technol. 29, 97–114 (2013)
6. Goverde, R. M. P., Scheepmaker, G. M., Wang, P.: Pseudospectral optimal train control. Eur. J. Oper. Res. 292(1), 353–375 (2021)
7. Howlett, P.: The optimal control of a train. Ann. Oper. Res. 98(1), 65–87 (2000)
8. Liu, R., Golovitcher, I. M.: Energy-efficient operation of rail vehicles. Transp. Res. A Policy Practice 37(10), 917–932 (2003)

9. Tian, Z., Zhao, N., Hillmansen, S., Roberts, C., Dowens, T., Kerr, C.: SmartDrive: Traction energy optimization and applications in rail systems. IEEE Trans. Intell. Transp. Syst. 20(7), 2764–2773 (2019)
10. Scheepmaker, G. M., Goverde, R. M. P.: The interplay between energy-efficient train control and scheduled running time supplements. J. Rail Transp. Plann. Manage. 5(4), 225–239 (2015)
11. Haahr, J. T., Pisinger, D., Sabbaghian, M.: A dynamic programming approach for optimizing train speed profiles with speed restrictions and passage points. Transp. Res. B: Methodol. 99, 167–182 (2017)
12. Xiao, Z., Wang, Q., Sun, P., Zhao, Z., Rao, Y., Feng, X.: Real-time energy-efficient driver advisory system for high-speed trains. IEEE Trans. Transp. Electrif. 7(4), 3163–3172 (2021)
13. Xing, Z., Zhang, Z., Guo, J., Qin, Y., Jia, L.: Rail train operation energy-saving optimization based on improved brute-force search. Appl. Energy 330, 120345 (2023)
14. Zhao, N., Tian, Z., Chen, L., Roberts, C., Hillmansen, S.: Driving strategy optimization and field test on an urban rail transit system. IEEE Intell. Transp. Syst. Mag. 13(3), 34–44 (2021)
15. ShangGuan, W., Yan, X. H., Cai, B. G., Wang, J.: Multiobjective optimization for train speed trajectory in CTCS high-speed railway with hybrid evolutionary algorithm. IEEE Trans. Intell. Transp. Syst. 16(4), 2215–2225 (2015)
16. Rao, Y., Sun, P., Wang, Q., Bai, B., Feng, X.: Optimal running time supplement for the energy-efficient train control considering the section running time constraint. IET Intel. Transp. Syst. 16(5), 661–674 (2022)
17. Albrecht, A., Howlett, P., Pudney, P., Vu, X., Zhou, P.: The key principles of optimal train control—Part 1: Formulation of the model, strategies of optimal type, evolutionary lines, location of optimal switching points. Transp. Res. B Methodol. 94, 482–508 (2016)
18. Albrecht, A., Howlett, P., Pudney, P., Vu, X., Zhou, P.: The key principles of optimal train control—Part 2: Existence of an optimal strategy, the local energy minimization principle, uniqueness, computational techniques. Transp. Res. B Methodol. 94, 509–538 (2016)
19. Wong, K. K., Ho, T. K.: Dynamic coast control of train movement with genetic algorithm. Int. J. Syst. Sci. 35(13–14), 835–846 (2004)
20. Yang, L., Li, K., Gao, Z., Li, X.: Optimizing trains movement on a railway network. Omega 40(5), 619–633 (2012)
21. Bocharnikov, Y., Tobias, A., Roberts, C., Hillmansen, S., Goodman, C.: Optimal driving strategy for traction energy saving on DC suburban railways. IET Electr. Power Appl. 1(5), 675–682 (2007)
22. Domínguez, M., Fernández-Cardador, A., Cucala, A. P., Gonsalves, T., Fernández, A.: Multi objective particle swarm optimization algorithm for the design of efficient ATO speed profiles in metro lines. Eng. Appl. Artif. Intell. 29, 43–53 (2014)
23. Ran, X. C., Chen, S. K., Liu, G., Bai, Y.: Energy-efficient approach combining train speed profile and timetable optimisations for metro operations. IET Intel. Transp. Syst. 14(14) 1967–1977 (2020)
24. Zixuan, Z., Yuan, C., Shuai, S.: Energy-efficient driving strategy for high-speed trains with considering the checkpoints. Chinese J. Electron. 32(5), 1 (2023)
25. Su, S., Zhu, Q., Liu, J., Tang, T., Wei, Q., Cao, Y.: A data-driven iterative learning approach for optimizing the train control strategy. IEEE Trans. Ind. Inf. 19(7), 7885–7893 (2023)
26. Su, S., Huang, Y., Liu, W., Tang, T., Cao, Y., Liu, H.: Optimization of the speed curve for heavy-haul trains considering cyclic air braking: an MILP approach. Eng. Optim. 55(5), 876–890 (2023)
27. Pröhl, L., Aschemann, H., Palacin, R.: The influence of operating strategies regarding an energy optimized driving style for electrically driven railway vehicles. Energies 14(3), 583 (2021)
28. Harrison, T. J., Midgley, W. J. B., Goodall, R. M., Ward, C. P.: Development and control of a rail vehicle model to reduce energy consumption and carbon dioxide emissions. Proc. Institut. Mech. Engineers, Part F: J. Rail Rapid Transit 235(10), 1237–1248 (2021)
29. Howlett, P., Milroy, I. P., Pudney, P.: Energy-efficient train control. Control Eng. Pract. 2, 193–200 (1994)
30. Domínguez, M., Fernández, A., Cucala, A. P., Lukaszewicz, P.: Optimal design of metro automatic train operation speed profiles for reducing energy consumption. Proc. Instit. Mech. Engineers, Part F: J. Rail Rapid Transit. 225(5), 463–473 (2011)
31. Pu, Q., Zhu, X., Liu, J., Cai, D., Fu, G., Wei, D., Sun, J., Zhang, R.: Integrated optimal design of speed profile and fuzzy PID controller for train with multifactor consideration. IEEE Access 8, 152146–152160 (2020)
32. Pu, Q., Zhu, X., Zhang, R., Liu, J., Cai, D., Fu, G.: Multiobjective optimization on the operation speed profile design of an urban railway train with a hybrid running strategy. IEEE Intell. Transp. Syst. Mag. 14(4), 230–243 (2022)
33. Carvajal-Carreño, W., Cucala, A. P., Fernández-Cardador, A.: Optimal design of energy-efficient ATO CBTC driving for metro lines based on NSGA-II with fuzzy parameters. Eng. Appl. Artif. Intell. 36, 164–177 (2014)
34. Li, S., Liu, R., Gao, Z., Yang, L.: Integrated train dwell time regulation and train speed profile generation for automatic train operations on high-density metro lines: A distributed optimal control method. Transp. Res. B Methodol. 148, 82–105 (2021)
35. Xing, C., Li, K., Zhang, L., Tian, Z.: Robust optimization of energy-saving train trajectories under passenger load uncertainty based on p-NSGA-II. IEEE Trans. Transp. Electrif. 9(1), 1826–1844 (2023)
36. Fernández-Rodríguez, A., Su, S., Fernández-Cardador, A., Cucala, A. P., Cao, Y.: A multi-objective algorithm for train driving energy reduction with multiple time targets. Eng. Optim. 53(4), 719–734 (2021)
37. Rochard, B. P., Schmid, F.: A review of methods to measure and calculate train resistances. J Proc. Instit. Mech. Engineers Part F J. Rail Rapid Transit. 214(4), 185–199 (2000)
38. Gu, Q., Tang, T., Cao, F., Song, Y. d.: Energy-efficient train operation in urban rail transit using real-time traffic information. IEEE Trans. Intell. Transp. Syst. 15(3), 1216–1233 (2014)
39. Nantomah, K.: Generalized Hölder's and Minkowski's inequalities for Jackson's q-integral and some applications to the incomplete q-gamma function. Abstr. Appl. Anal. 2017, 9796873 (2017)
40. Feng, M., Wu, K., Lu, S.: A fast-solved model for energy-efficient train control based on convex optimization. *arXiv preprint arXiv:2201.10731* (2022)
41. Zhu, Q., Su, S., Tang, T., Liu, W., Zhang, Z., Tian, Q.: An eco-driving algorithm for trains through distributing energy: A Q-Learning approach. ISA Trans. 122, 24–37 (2022)
42. Wu, C., Xu, B., Lu, S., Xue, F., Jiang, L., Chen, M.: Adaptive eco-driving strategy and feasibility analysis for electric trains with onboard energy storage devices. IEEE Trans. Transp. Electrif. 7(3), 1834–1848 (2021)
43. Feng, M., Huang, Y., Lu, S.: Eco-driving strategy optimization for high-speed railways considering dynamic traction system efficiency. IEEE Trans. Transp. Electrif. 1–1 (2023)

How to cite this article: Liu, X., Tian, Z., Jiang, L., Lu, S., Zeng, P.: An improved energy-efficient driving strategy for routes with various gradients and speed limits. IET Intell. Transp. Syst. 1–15 (2024). https://doi.org/10.1049/itr2.12482